Proceedings of IMECE2002
ASME International Mechanical Engineering Congress & Exposition
November 17–22, 2002, New Orleans, Louisiana

IMECE2002-39309

MICRO-ELECTROSTATIC VIBRATION-TO-ELECTRICITY CONVERTERS

Shad Roundy
Department of Mechanical Engineering
2111 Etcheverry Hall
Berkeley, CA 94720, USA
shadr@kingkong.me.berkeley.edu

Paul K. Wright
Department of Mechanical Engineering
5133 Etcheverry Hall
Berkeley, CA 94720, USA
pwright@kingkong.me.berkeley.edu

Kristofer S. J. Pister
Department of Electrical Engineering
497 Cory Hall
Berkeley, CA 94720, USA
pister@eecs.berkeley.edu

ABSTRACT

Advances in low power VLSI design, along with the potentially low duty cycle of wireless sensor nodes open up the possibility of powering small wireless computing devices from scavenged ambient power. Low level vibrations occurring in typical household, office, and manufacturing environments are considered as a possible power source for wireless sensor nodes. This work focuses on the design of electrostatic vibration-to-electricity converters using MEMS fabrications technology. Detailed models of three different design concepts are developed. The three design concepts are evaluated and compared based on simulations and practical considerations. A formal optimization of the preferred design concept is performed, and a final design is produced using the optimal design parameters. Simulations of the optimized design show that an output power density of 116 μW/cm^3 is possible from input vibrations of 2.25 m/s^2 at 120 Hz. Test devices have been designed for a Deep Reactive Ion Etching (DRIE) process that etches MEMS structures into the top layer of a Silicon On Insulator (SOI) wafer. The devices are currently being fabricated.

KEYWORDS: energy scavenging; vibration to electricity conversion

1. INTRODUCTION

The past few years have seen in increasing focus on the development of networks of wireless sensor nodes [1]. Applications for ubiquitous wireless sensor networks range from environmental monitoring and control of industrial buildings to aerospace and military applications. Advances in low power VLSI design and CMOS fabrication [2] have reduced power requirements for wireless sensor nodes to the point that self-powered nodes are now feasible. Using current state of the art technology, a low duty cycle wireless sensor device could dissipate as little power as tens to hundreds of microwatts and be as small as one cubic centimeter.

Many methods to harvest or scavenge energy from the environment for use by low power electronics have been considered. Perhaps the most widely used and most mature method to scavenge energy is photovoltaic cell. In direct sunlight, a silicon solar cell of average efficiency can produce about 15 mW/cm^2. However, in normal office lighting, the same solar cell will only produce about 10 μW/cm^2. Solar cells are very good when sufficiently intense light is available, but are inadequate in many applications. Stordeur and Stark have demonstrated a thermoelectric micro-device capable of converting 15 μW/cm^3 from a 10 °C temperature gradient [3]. Devices to convert vibrations to electricity have also been designed and tested. Williams and Yates [4] have demonstrated 0.3 μW of power from a device that measured 4mm X 4mm X 1mm, which translates to a power density of about 10 μW/cm^3. Meninger et al. [5] have designed a device that is capable of 3.8 μW/cm^3 according to simulations. The authors' own calculations show that power densities on the order of 100 μW/cm^3 should be possible from commonly occurring vibration sources. Table 1 shows a comparison of various different energy scavenging techniques. The source of the data is shown in the far right column. All values are normalized by volume, and are reported as μW/cm^3.

Copyright © 2002 by ASME

	Power Density ($\mu W/cm^3$)	Source of information
Solar (Outdoors)	15,000 - direct sun 150 - cloudy day	Commonly Available
Solar (Indoors)	6 - office desk	Experiment
Vibrations	100	Experiment & Theory
Acoustic Noise	0.003 @ 75 Db 0.96 @ 100 Db	Theory
Daily Temp. Variation	10	Theory
Temp. Gradient	15 @ 10 ºC gradient	[3]
Shoe Inserts	330	[6]

Table 1. Comparison of energy scavenging sources

Advances in energy storage devices such as primary batteries may allow a wireless sensor node to be powered for a very long time, perhaps its entire lifetime. Table 2 summarizes the energy density of available from several energy storage devices. The middle column of the table gives the average amount of power available over a 1 year lifetime, and the right hand column gives the average amount of power continuously available over a 10 year lifetime. Battery leakage was included. Efficiencies used for heat engines and fuel cells are 80% and 40% respectively. Both micro heat engines and micro fuel cells are still in the research stage. The data in Table 2 show that for lifetimes of about 1 to 3 years, an energy storage device could likely supply enough average power to operate a wireless sensor node. However, for longer projected lifetimes, a truly self-sustaining power source would be necessary.

	Power Density ($\mu W/cm^3$) 1Year lifetime	Power Density ($\mu W/cm^3$) 10 Year lifetime
Batteries (non-recharg. Lithium)	90	7
Batteries (rechargeable Lithium)	15	0
Micro Heat Engine (hydrocarbon fuel)	320	32
Fuel Cells (methanol)	220	22

Table 2. Comparison of energy storage technologies

Commonly occurring vibrations are a potentially useful method of powering wireless sensor nodes or other small computing devices that need their own power source. Although vibrations are available only in certain environments, there are a substantial number of application areas in which sufficient vibration energy exists. Application areas include spaces with industrial equipment such as manufacturing or automated assembly floors, certain locations in buildings such as the heating and cooling ducts, small appliances, large exterior windows, automobiles, aircraft, etc. The authors therefore have undertaken a detailed study of the use of vibrations as a power source for small computing and communication devices.

Three possible methods of converting mechanical vibration energy to electricity exist: electromagnetic, electrostatic, and piezoelectric conversion. Williams and Yates [4] have designed and built a micro-electromagnetic converter. Their chief contribution, in addition to the development of the electromagnetic generator, was the development of a generic second order linear model for power conversion. It turns out that this model fits electromagnetic conversion very well, and they showed close agreement between the model and experimental results. However, they drove the converter with vibrations of 500 nm magnitude at 4.4 kHz, which are far more energetic and of far higher frequency than those measured in common environments. Secondly, although the output voltage of the converter is not reported, calculations made by the authors show that the output voltage is about 8 mV AC. This presents serious problems since the AC power source would need to be transformed up 2 to 3 orders of magnitude before it could be rectified and conditioned for use by standard electronics. In fact, it can easily be shown that with current fabrication techniques and realistic vibration sources, output voltages above 100 mV from an electromagnetic converter of size 1 cm^3 are not possible. Amirtharajah and Chandrakasan [7] also built an electromagnetic converter with custom designed power electronics and actually used it to power a custom low power DSP. The converter size is 4 cm X 4 cm X 10 cm. The maximum output voltage was 180 mV necessitating a 10 to 1 transformer in order to rectify the voltage.

Piezoelectric material can also be used as a means to convert vibrations to electric power. The authors are not aware of any research in this area. They are currently conducting research in this area. Elvin et. al. [8] have designed a self powered strain sensor that wirelessly transmits its data. The straining of the piezoelectric sensor is used as a means to power the electronics. While there are obvious differences between this self-powered strain sensor and a vibration-to-electricity converter, there are also many similarities. Schmidt [9] has investigated the use of piezoelectric polymer for use in power generating windmills. Again, there are many similarities, but also many differences between Schmidt's work and a vibration-to-electricity converter.

This paper will focus on the design of electrostatic vibration-to-electricity converters. Electrostatic converters have the advantage that they can be more easily implemented with MEMS technology. The ability to fabricate the converters with silicon based MEMS technology improves the level of integration possible with silicon based microelectronics. Furthermore, voltages within the usable range can be generated obviating the need for a large and expensive transformer. Meninger et al. [5] have designed an electrostatic converter fabricated with MEMS technology. Their simulations show that 8.6 μW can be converted from a device 1.5 cm X 1.5 cm in size. The actual measured power output is not reported. One of the group's largest contributions is the development of power electronics for use with the converter. They are also the first to publish a design for an electrostatic vibration-to-electricity converter. The work reported in this paper aims to cover the topic of electrostatic vibration-to-electricity converters based on MEMS technology in greater detail. First, the features of common vibration sources, for which the MEMS devices will be designed, will be considered. A comparison of different design concepts will then be presented. Detailed models and simulations are used to quantitatively compare the different design concepts. Finally, an optimized design will be presented along with simulation results.

Copyright © 2002 by ASME

2. COMMON VIBRATION SOURCES

Many commonly occurring vibration sources have been measured and characterized by the authors. Figure 1 shows the spectra of two vibrations sources: the casing of a microwave oven and the base of a milling machine. Other vibration sources measured include a notebook computer casing, cooling ducts, large exterior windows, the floor in high traffic areas of office buildings, and several household appliances.

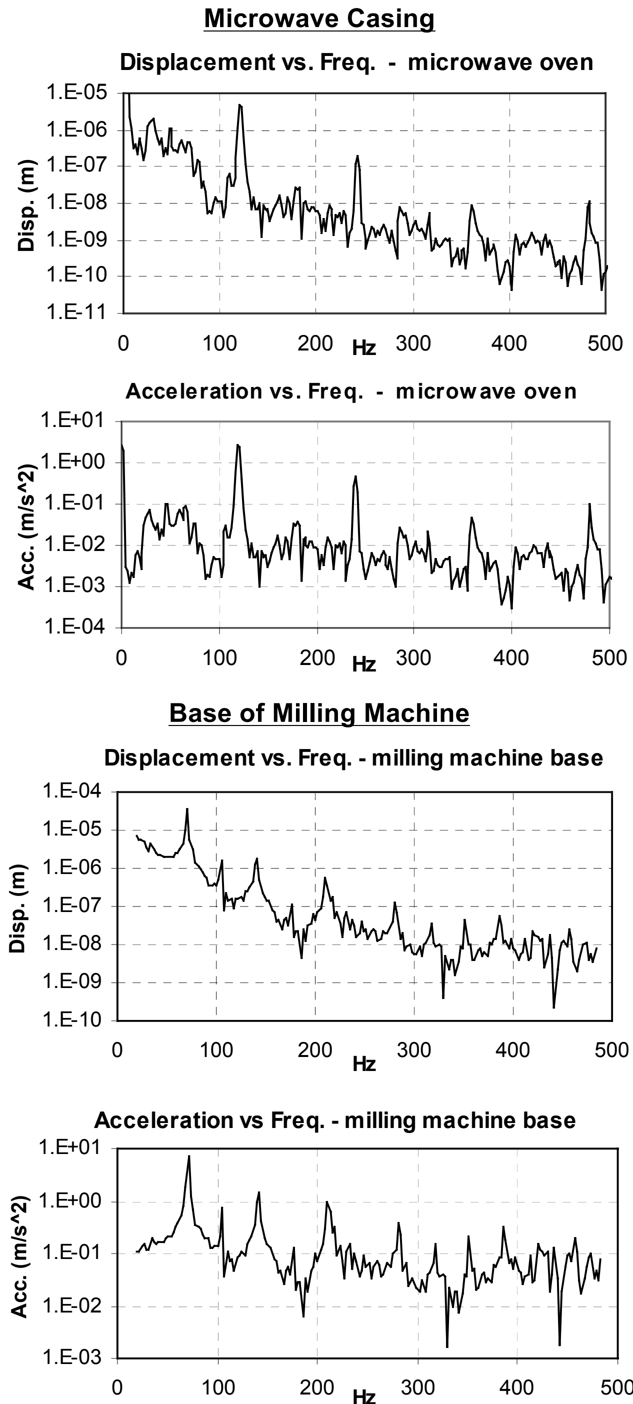

Figure 1. Vibration spectra for a microwave oven casing and the base of a milling machine. Figure shows both the displacement and acceleration magnitudes of the vibration sources vs. frequency.

The top graph shows displacement magnitude versus frequency, and the bottom graph shows acceleration magnitude versus frequency. Two important characteristics that are common to virtually all of the sources measured are: a) there is a large peak in magnitude somewhere below 200 Hz, which can be referred to as the fundamental mode, and b) the acceleration spectrum is relatively flat with frequency, which means that the displacement spectrum falls of as $1/\omega^2$. These two characteristics are clearly visible in the plots shown in Figure 1.

Information about the potential vibration sources is important to the design of vibration converters for at least three reasons. First, an assumption of steady state vibrations concentrated at one frequency appears reasonable based on the measured spectra. Second, the higher frequency vibration modes are lower in acceleration magnitude than the low frequency fundamental mode. This fact means that the most energetic mode is the lowest frequency mode, and that the converter should be designed to resonate at this frequency. Third, in order to estimate the potential power generation, the magnitude and frequency of the driving vibrations must be known. Finally, it should be noted that the vibrations from the microwave oven, whose potential for energy conversion falls about in the middle of all the sources measured, have been used as a basis for the simulations and design of actual devices that will be presented later.

3. GENERALIZED CONVERSION MODEL

The basis of electrostatic energy conversion is the variable capacitor. The variable capacitance structure, which will be fabricated with MEMS technology, is driven by mechanical vibrations and oscillates between a maximum capacitance (C_{max}) and a minimum capacitance (C_{min}). If the charge on the capacitor is constrained, the voltage will increase as the capacitance decreases. If the voltage across the capacitor is constrained, charge will move from the capacitor to a storage device or to the load as the capacitance decreases. In either case, mechanical kinetic energy is converted to electrical energy. Meninger et. al. [5] give a good explanation of the merits of charge constrained conversion versus voltage constrained conversion. This project will work with charge constrained converters because two separate voltage sources are needed for voltage constrained conversion.

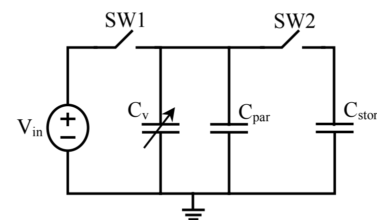

Figure 2. Simple circuit representation for an electrostatic converter.

A simplified circuit for an electrostatic generator using charge constrained conversion is shown in Figure 2. This circuit is useful for power output calculations and demonstrates the basic function of energy conversion although it is not entirely realistic. A pre-charged reservoir, which could be a capacitor or rechargeable battery, is represented as the input voltage source V_{in}. The variable capacitor C_v is the MEMS

Copyright © 2002 by ASME

structure and C_{par} is the parasitic capacitance associated with the MEMS structure and any interconnections. When C_v is at C_{max}, switch 1 (SW1) closes, and charge is transferred from the input to the variable capacitor. The MEMS structure then moves from its maximum capacitance position to the minimum capacitance position with both switches open. The increase in energy stored on the capacitor is given by expressions in Eq. (1a) and (1b).

$$E = \frac{1}{2} V_{in}^2 (C_{max} - C_{min}) \left(\frac{C_{max} + C_{par}}{C_{min} + C_{par}} \right) \quad (1a)$$

$$E = \frac{1}{2} V_{max} V_{in} (C_{max} - C_{min}) \quad (1b)$$

The term V_{max} in Eq. (1b) represents the maximum allowable voltage across a switch. Depending on the specific circuit implementation, this may be very limiting constraint. If the conversion is constrained by the maximum allowable voltage, the form of Eq. (1b) is the more useful. At minimum capacitance, switch 2 (SW2) closes and the charge stored on C_v (now in a higher energy state) is transferred onto the storage capacitor C_{stor}. The mechanical vibrations have done work on the MEMS variable capacitor causing an increase in the total energy stored in the system.

In reality, the switches would either be diodes, or transistors with an inductor, and some method of returning a portion of the charge put onto the storage capacitor to the input reservoir would need to be employed. Again, Meninger et al. [5] have detailed a circuit to accomplish this task. However, the circuit shown in Figure 2 is sufficient for the analysis presented in this paper.

It is important to note that actual travel of the variable capacitance structure, and therefore the value of C_{max} and C_{min}, is determined by both the mechanical dynamics of the system and the design of the MEMS structure. A schematic of the mechanical system is shown in Figure 3. Two nonlinear dampers are shown. The damper on the right, shown by the term $b_m(z,\dot{z})$, is a function of the spring deflection z, and the time derivative of the spring deflection. The exact form of the expression depends on the type of structure designed, but in all cases it represents energy lost due to fluid damping. The damper on the left is an electrically induced damping that represents energy removed from the mechanical subsystem and stored in the electrical subsystem. Again, the exact expression depends on the details of the implementation.

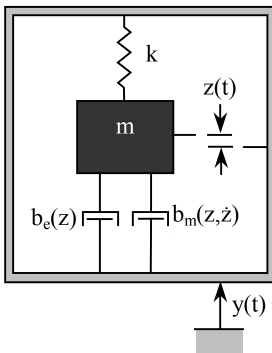

Figure 3. Mechanical schematic of MEMS structure.

The equation of motion for the mechanical system shown in Figure 3 is shown in Eq. (2) where m is the mass of the oscillating MEMS structure, k is the stiffness of flexures attached to the structure, z is the deflection of the flexures, y is the input vibration signal, $b_m(z,\dot{z})$ is the fluid damping force, and $b_e(z)$ is the electrostatic force induced on the MEMS structure. The capacitance of the MEMS variable capacitor at a given time (t) is determined by the deflection of the flexure (z) and the specifics of the design.

$$m\ddot{z} + b_e(z) + b_m(z,\dot{z}) + kz = -m\ddot{y} \quad (2)$$

The amount of energy per cycle that is removed from the mechanical system, and stored in the electrical system is given by

$$E = \int_0^{2\pi/\omega} b_e(z)\,dz \quad (3)$$

where ω is the frequency of oscillation. The expression for energy per cycle given by Eq. (3) is equivalent to that shown in Eq. (1a). Consider a simple example of a variable capacitor consisting of two square plates. The capacitor changes capacitance as one plate, attached to springs, oscillates between values z_{min} and z_{max} where z is the distance between the two plates. The form of $b_e(z)$ for this example is

$$b_e(z) = \frac{Q^2}{2\varepsilon_0 A} \quad (4)$$

where Q is the charge on the capacitor, which is constrained to be constant, ε_0 is the dielectric constant of free space, and A is the area of the capacitor plates. Note that for this example, $b_e(z)$ is constant and not a function of z, however this is not always the case. Substituting Eq. (4) into Eq. (3) and solving yields the following expression:

$$E = \frac{Q^2}{2\varepsilon_0 A}\left(z_{max} - z_{min}\right) \quad (5)$$

In deriving Eq. (5) it was assumed that all the charge is removed from the variable capacitor as it returns from the C_{min} (or z_{max}) state back to the C_{max} (or z_{min}) state. Noting that $C_{max}=\varepsilon_0 A/z_{min}$, $C_{min}=\varepsilon_0 A/z_{max}$, and $Q=C_{max}*V_{in}$, Eq. (5) can be easily reduced to

$$E = \frac{1}{2} V_{in}^2 \left(C_{max} - C_{min}\right)\left(\frac{C_{max}}{C_{min}}\right) \quad (6)$$

which is the same expression as Eq. (1a) neglecting the parasitic capacitance. Note also that ($z_{max} - z_{min}$) is nothing more than the AC magnitude of z (the distance between plates). If it is assumed that the mechanical damping is linear viscous damping ($b_m\dot{z}$), then the AC magnitude of z is given by

$$|Z| = \frac{m\omega}{b_m}|Y| \quad (7)$$

where |Y| is the magnitude of the input vibrations, m is the mass of the variable capacitor structure, b_m is a constant damping coefficient, and ω is assumed to be equal to the natural frequency (ω_n) of the mass spring structure.

Copyright © 2002 by ASME

Substituting Eq. (7) into Eq. (5) yields:

$$E = \frac{m\omega Q^2}{2b_m\varepsilon_0 A}|Y| \quad (8)$$

Eq. (8) clearly shows that the energy converted per cycle is linearly proportional to the mass of the system. Therefore, maximizing the mass of the system becomes an important design consideration.

4. FABRICATION PROCESS

Two primary considerations greatly affected the choice of fabrication process. As can be easily seen from Eqs. (1a) and (1b), the energy output per cycle is highly dependent on the maximum capacitance of the MEMS structure. Devices fabricated by standard surface micromachining techniques are generally only one to several μm thick, and thus do not generate very large capacitances. Thick structures with high aspect ratios are preferable for generating large capacitances. Secondly, as shown above, the potential power output is linearly proportional to the mass of the oscillating device. As silicon is not a dense material, and MEMS structures are typically not very thick, the mass of the structure itself will be very small. Significantly more power can be generated if a large mass made of a dense material is attached to the structure after fabrication. Again, thick structures are desirable in order to support a larger proof mass. For these two reasons, a Deep Reactive Ion Etching (DRIE) process was selected so that very thick structures can be etched into a Silicon On Insulator (SOI) wafer. The basics of the process chosen to create the variable capacitance structure are shown in Figure 4.

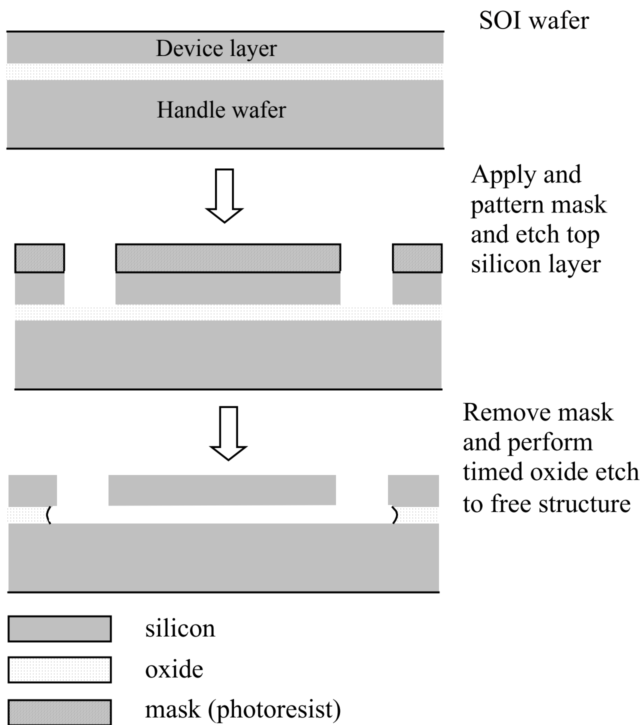

Figure 4. DRIE process with SOI wafer used to create variable capacitance structure.

Close integration with at least switches SW1 and SW2 in Figure 2 is important in order to minimize the parasitic capacitance. Two methods of integrating the switches on the same die with the MEMS structure are being pursued. The first utilizes a process that fabricates diodes and high voltage MOSFETS on the SOI wafer before etching and releasing the MEMS structures. The second approach is to assemble bare die diodes directly on the MEMS chip. Gold pads are patterned on the MEMS die. Solder is then applied to the gold pads. The bare die diodes are then attached to the solder bumps by a fluidic self-assembly process [10] after which the solder is reflowed to create a good electrical connection. Devices using both of these approaches are currently in fabrication.

5. EXPLORATION OF DESIGN CONCEPTS AND DEVICE SPECIFIC MODELS

Three basic topologies for micromachined variable capacitors are shown in Figure 5.

Figure 5a, In-plane overlap type:
Capacitance changes by changing overlap area of fingers. (Not to scale)

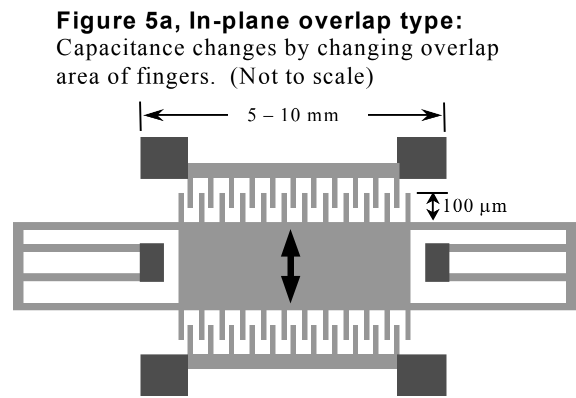

Figure 5b, In-plane gap closing type:
Capacitance changes by changing gap between fingers. (Not to scale)

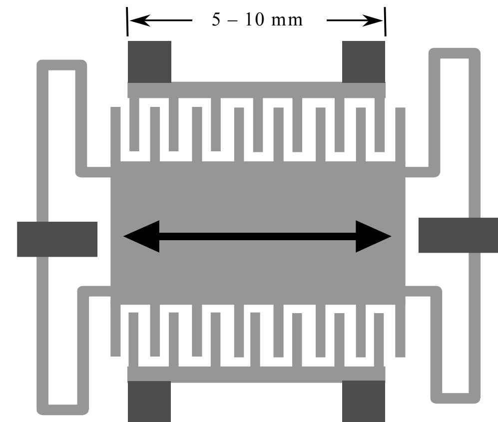

Figure 5c, Out-of-plane gap closing type:
Capacitance changes by changing gap between two large plates. (Not to scale)

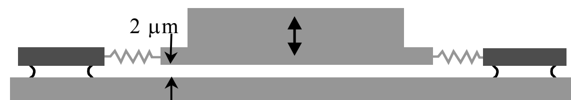

Figure 5. Three topologies for micromachined electrostatic converters.

Copyright © 2002 by ASME

The dark areas are fixed by anchors to the substrate, while the light areas are released structures that are free to move. The device shown in Figure 5a will be referred to as an in-plane overlap converter because the change in capacitance arises from the changing overlap area of the many interdigitated fingers. As the center plate moves in the direction shown, the overlap area, and thus the capacitance, of the fingers changes. Figure 5b will be referred to as an in-plane gap closing converter because the capacitance changes due to the changing dielectric gap between the fingers. The device shown in Figure 5c will be referred to as an out-of-plane gap closing converter. Note that the figure shows a top view of the first two devices, and a side view of the third device. This third device oscillates out of the plane of the wafer, and changes its capacitance by changing the dielectric distance between two large plates. A few representative dimensions are shown in the figure.

5.1 Out-of-plane gap closing converter

The out-of-plane gap closing type converter will be considered first. The exact expression for the mechanical damping term is give by

$$b_m(z,\dot{z}) = \frac{16\mu W^3 L}{z^3}\dot{z} \tag{9}$$

where μ is the viscosity of air, W is the width of the large plate, and L is the length of the plate. Note that the interpretation of z in this equation is slightly different than as shown in Figure 3 in that z represents the separation of the two plates making up the capacitor. Thus z is the sum of the initial separation and the deflection of the flexures. The capacitance of this structure is given by

$$C_v = \frac{\varepsilon_0 WL}{z} \tag{10}$$

where ε_0 is the dielectric constant of free space. Finally, the expression for the electrostatic force induced is given by

$$b_e(z) = \frac{-Q^2}{2\varepsilon_0 WL} \tag{11}$$

where Q is the charge on the variable capacitor. Because the charge is held constant during the motion of the structure, the electrostatic force is constant. When the switches close, the amount of charge on the capacitor changes, but this happens very fast and can be considered to be instantaneous from the viewpoint of the mechanical subsystem.

Eqs. (9-11) demonstrate one of the problems with the out-of-plane gap closing converter. In order to obtain a large capacitance change, z must become very small, or the plates must move very close together. However, as the fluid damping force is proportional to $1/z^3$, the loss becomes very large as the plates move close together. This problem may be alleviated somewhat by packaging the device under very low pressure. However, another serious problem exists with this design concept. As the plates get close together, surface interaction forces will tend to make them stick together shorting the circuit and possibly becoming permanently attached. It is very difficult to design mechanical stops to prevent this from happening with the out-of-plane topology.

5.2 In-plane gap closing converter

The in-plane gap closing converter considerably improves the latter problem mentioned with the out-of-plane converter. Because the motion is now in the plane of the wafer, mechanical stops can be easily incorporated with standard fabrication processes, and therefore, the minimum dielectric gap, and thus the maximum capacitance can be precisely controlled. The expression for the fluid damping term for the in-plane gap closing type converter is given by

$$b_m(z,\dot{z}) = \left(\frac{\mu A}{d_0} + \frac{8\mu N_g L_f h^3}{(z-d)^3}\right)\dot{z} \tag{12}$$

where A is the area of the center plate, d_0 is the vertical distance between the center plate and the substrate underneath, N_g is the number of gaps formed by the interdigitated fingers, L_f is the length of the fingers, h is the thickness of the device, and d is the initial gap between fingers. Note that z in this expression is the deflection of the flexures. The capacitance of the structure is given by:

$$C_v = N_g \varepsilon_0 L_f h\left(\frac{2d}{d^2 - z^2}\right) \tag{13}$$

The expression for the electrostatic force induced is given by:

$$b_e(z) = \frac{Q^2 z}{2N_g d\varepsilon_0 L_f h} \tag{14}$$

Note that the electrostatic force is proportional to the deflection of the flexure, and thus acts much like a mechanical spring except that the electrostatic force operates in the opposite direction.

While the fluid damping is still quite high for this design, large differences in capacitance can be generated and precise control of the maximum capacitance is possible if mechanical stops are included in the design.

5.3 In-plane overlap converter

The expression for fluid damping for the overlap in-plane converter is

$$b_m = \frac{N_g \mu L_f h}{d}\dot{z} \tag{15}$$

where d is the dielectric gap between fingers. Eq. (15) is actually in the standard form for linear viscous damping. The capacitance for the structure is given by

$$C_v = \frac{N_g \varepsilon_0 L_f (z + z_0)}{d} \tag{16}$$

where z_0 is the initial overlap distance of interdigitated fingers. The expression for the electrostatic force induced is given by

$$b_e(z) = \frac{Q^2 d}{2N_g \varepsilon_0 h(z+z_0)^2} \tag{17}$$

5.4 Initial Comparison

A useful comparison between in-plane overlap and gap closing converters can be made without performing simulations that take into account the full dynamics of the systems. Estimates of power output per cm^3 based only on geometry and the relationship in Eq. (1a) are graphed against maximum flexure (spring) deflection in Figure 6. The input voltage used for this comparison was 5 volts. It should be noted that for the in-plane gap closing converter the number of fingers that can be fabricated is a function of the maximum deflection of the

Copyright © 2002 by ASME

flexures because the fingers must be spaced far enough apart to accommodate the displacement. Therefore a higher spring deflection results in a lower maximum (and minimum) capacitance. This is not true for in-plane overlap converters. The result is that for in-plane overlap converters a larger spring deflection always results in more power out. However, there is an optimal travel distance for in-plane gap closing converters as can be seen Figure 6. While both types of converters are capable of roughly the same power output, this power output occurs at very large spring deflections for the overlap converter. Such large spring deflections raise concerns about the stability of the system. This point will be examined in more detail in the following section while considering dynamic simulations of the system. As a final item of comparison, the gap closing converter is far less sensitive to the parasitic capacitance. Remember that this comparison does not take into the dynamics of the system into consideration, and it therefore assumes that the spring deflections used to calculate the maximum and minimum capacitances can in fact be obtained from the driving vibrations. While this may not always be a valid assumption, the features of the two designs discussed above are still valid. Detailed dynamic simulation of the systems will be presented in the following section.

In-plane overlap converter

Power / cm^3 vs. Spring Deflection

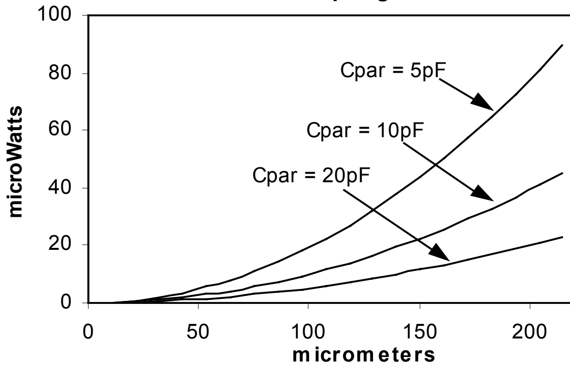

In-plane gap closing converter

Power / cm^3 vs. Spring Deflection

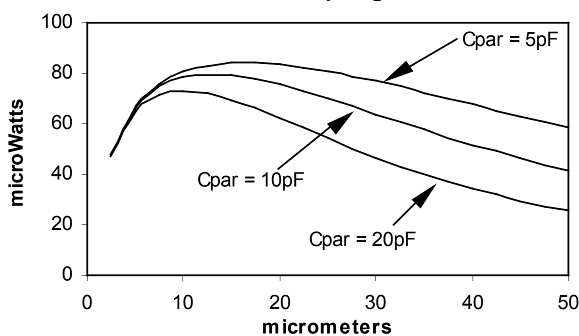

Figure 6. Power density vs. flexure deflection for in-plane overlap and gap closing converters for three different values of parasitic capacitance.

6. SIMULATION RESULTS

All dynamic simulations were performed in Matlab based on Eqs (1a, 2, 9-17). A space constraint of 1cm^3 was placed on the device size for all simulations. Thus the results are normalized as power per cubic centimeter. Simulation results will be presented for all three design topologies in order to more fully compare the merits of each converter type.

6.1 Simulations - out-of-plane gap closing converter

Simulation results for out-of-plane gap closing type converter will be presented first. Figure 7 shows the voltage on the output capacitor and the voltage on the MEMS variable capacitor vs. time. The traces in Figure 7 demonstrate the basic charge pump function of the simple simulation circuit shown in Figure 2. This simulation was performed with an input voltage of 5 volts, a storage capacitor of 100 pF, an ambient pressure of 0.01 atmospheres, and a parasitic capacitance of 20 pF. The switches are assumed to be ideal in that they turn on and off instantaneously and switching loss is neglected.

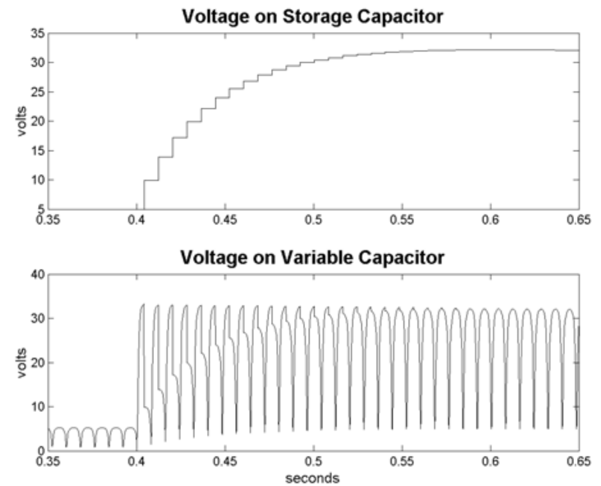

Figure 7. Voltage on storage capacitor and variable capacitor vs. time.

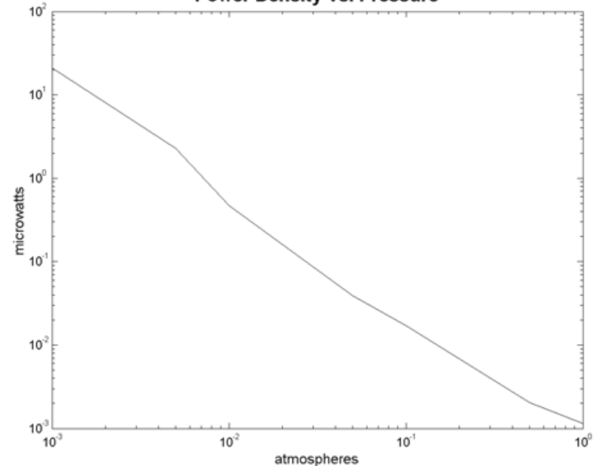

Figure 8. Power per cm^3 vs. pressure.

Copyright © 2002 by ASME

As discusses earlier, the out-of-plane topology suffers from very high squeeze film damping forces. At atmospheric pressure these damping forces dominate the system, and so most of the kinetic energy of the system is lost and very little power output is available. As various methods do exist to package MEMS structures at reduced pressures [11, 12], the system was simulated at a variety of different pressures. Figure 8 shows the output power per cm^3 vs. pressure in atmospheres. At .001 atmospheres (or 0.76 torr), the power output is 20 $\mu W/cm^3$, which may be in the useful range. At atmospheric pressure the power output is on the order of 1 nW/cm^3, which is far too low to be of any use.

6.2 Simulations – in-plane gap closing converter

A critical parameter for in the design of in-plane gap closing converters is the placement of the mechanical stops that determine the minimum dielectric gap between the interdigitated fingers. The maximum capacitance of the structure and the damping characteristics are determined by the choice of the minimum dielectric gap. Figure 9 shows the simulated power per cm^3 for an in-plane gap closing converter plotted against the minimum dielectric gap allowed. All other design parameters were held constant for this simulation. The device thickness was 100 μm, the parasitic capacitance was 20 pF, the initial gap between fingers was 22 μm, and the input voltage was 5v. Figure 9 highlights the fact that the minimum dielectric gap has a large effect on potential power output. The minimum dielectric gap that can be consistently achieved is not known and will require some experimentation. Prototypes with minimum gaps of 0.25 μm, 0.5 μm and 1μm are currently being fabricated. Simulations show that approximately 50 $\mu W/cm^3$ can be achieved with a dielectric gap 0.25 μm. Even at a minimum gap of 0.5 μm, approximately 20 μW can be generated, which is about the same as the out-of-plane converter at a pressure 0.001 atmospheres.

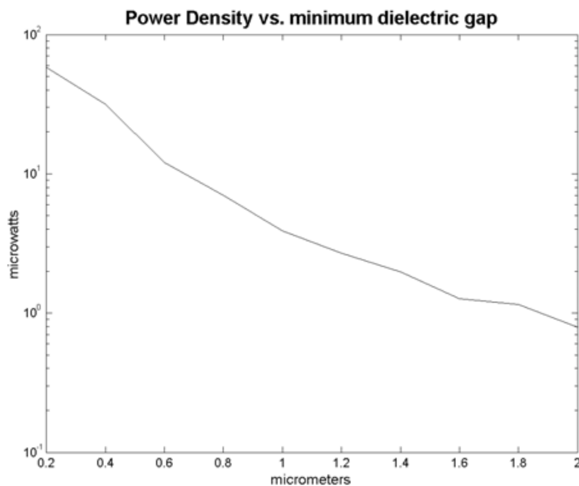

Figure 9. Power per cm^3 vs. minimum dielectric gap for in in-plane gap closing converter.

Figure 10 plots power per cm^3 against initial gap designed between fingers. This is basically the same plot as that shown in Figure 6 since the spring deflection is determined by the combination of the initial gap and the minimum gap. However, unlike the data shown in Figure 6, Figure 10 presents the results of a full dynamic simulation. Note that, as shown in Figure 6, there is an optimal initial gap (or spring deflection). However, in this case the output power is a little lower due to the realities of the mechanical dynamics.

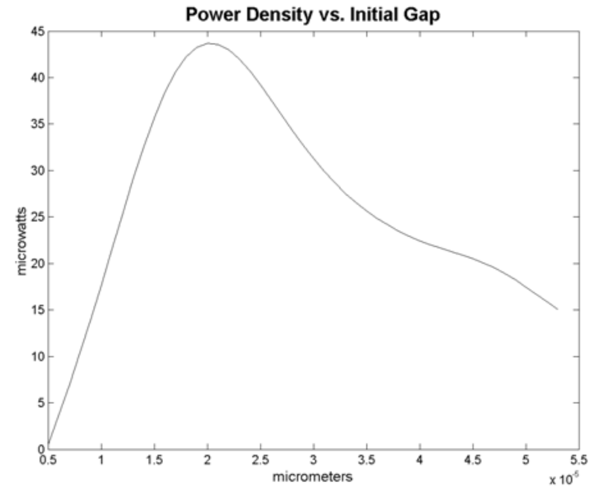

Figure 10. Power per cm^3 vs initial dielectric gap between fingers for in-plane gap closing converter.

6.3 Simulations – in-plane overlap converter

Unlike in-plane gap closing converters, in-plane overlap converters produce more output power at higher deflections. The actual magnitude of the deflections are determined by the dynamics of the system. While the magnitude of the deflections can be influenced in part by design parameters, it is largely a function of the magnitude and frequency of the input vibrations and the size constraint (1 cm^3 in this case), which determines the maximum mass. The length of the dielectric gap between the interdigitated fingers is a key design parameter for in-plane overlap converters. The maximum capacitance, and therefore the maximum output power, is largely affected by the gap between fingers. The minimum possible dielectric gap will be determined by the fabrication process and the thickness of the device layer. However, the stability of the system is a second issue that will affect the dielectric gap designed. If the deflections are very large (on the order of 100 μm) and the gap is very small (on the order of 1 μm), only a small moment induced by out-of-axis vibrations would be necessary to cause the fingers to touch and short the circuit. This potential problem is illustrated in Figure 11. Although there is no precise formula to determine how large the dielectric gap should be for a given amount of spring deflection, it seems likely that the stability issue will drive the dielectric gap to be designed larger than the minimum possible due to fabrication constraints.

Copyright © 2002 by ASME

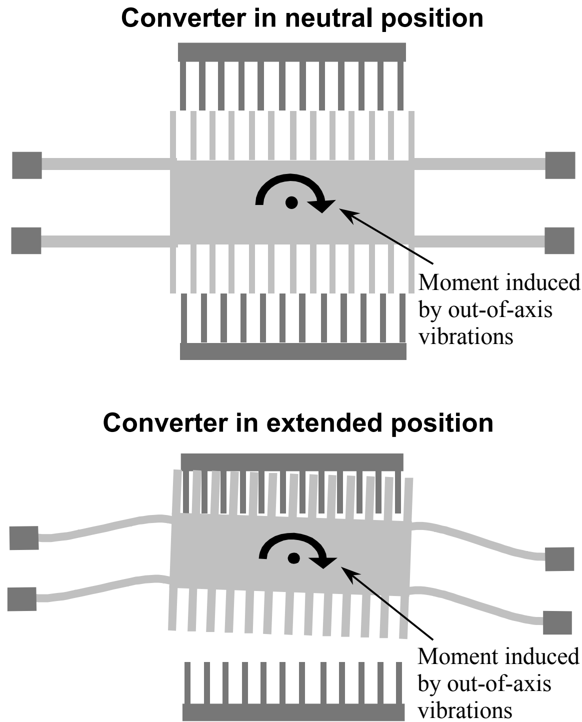

Figure 11. Illustration of stability problem with in-plane overlap design.

Figure 12 shows the maximum simulated power density versus the dielectric gap for an in-plane overlap converter. The device thickness was 50 μm, the parasitic capacitance was 20 pF, the input voltage was 5v, and the maximum aspect ratio allowed for features was 50 (which is in keeping with the fabrication process chosen).

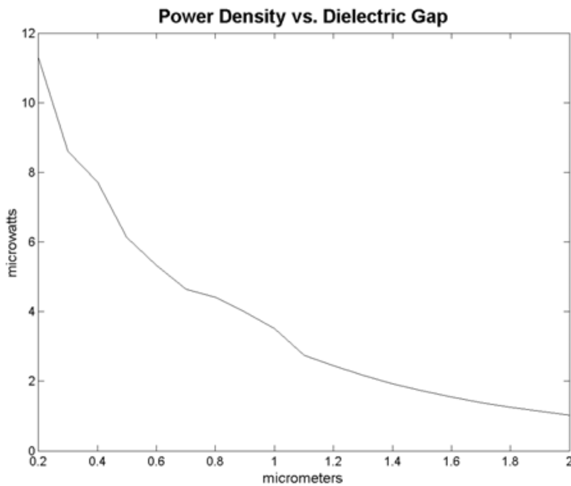

Figure 12. Power per cm^3 vs. dielectric gap between fingers for an in-plane overlap converter.

It is interesting to note that the maximum spring deflection for these simulations ranged from 162 to 164 μm and is primarily a function of the magnitude of the input vibrations and the amount of fluid damping. Given the input vibrations used (2.25 m/s^2 at 120 Hz) and a realistic level of fluid damping, larger spring deflections are not possible. For this reason, the maximum power level is significantly lower than that shown in Figure 6, which does not include the affect of input vibrations, limited mass, or damping. Even if larger deflections were possible, it is unlikely that a device with a ½ or ¼ μm dielectric gap could function in a stable manner with maximum deflections of 100 to 200 μm.

7. COMPARISON OF DESIGN CONCEPTS AND DESIGN OPTIMIZATION

The simulations presented in the previous section indicate that the highest power density is available from in-plane gap closing converters, followed by out-of-plane gap closing converters, and finally by in-plane overlap converters. Design parameters for the above simulations have been chosen to represent reasonable designs based upon engineering judgment. Fully optimized sets of design parameters, however, would yield devices capable of producing more power. While the above simulations are not absolute optimal designs, they do indicate that in-plane gap closing converters exhibit the highest power density. Furthermore, two previously mentioned practical problems exist with the two competing design concepts. The first is the potential stability problem with in-plane overlap converters. The second is that in an out-of-plane gap closing device like the one simulated, surface interaction forces will likely cause the two plates to stick together. Mechanical stops would need to be incorporated to keep the plates from sticking together and shorting the circuit. However, effective mechanical stops are difficult to incorporate in an out-of-plane design because of the lack of geometric freedom microfabrication processes allow in the vertical direction. Therefore, the in-plane gap closing design is clearly the preferable design based on both a quantitative and qualitative comparison.

Using the in-plane gap closing topology as the preferred concept, a more detailed design optimization can be done. There are certain physical constraints that limit the design space. First, the total volume of the device must be less the 1 cm^3. This will limit the total system mass, and thus the maximum achievable power output. A second constraint is the maximum aspect ratio of features. The silicon DRIE process for which this converter is designed has a maximum aspect ratio of about 50.

The following design parameters can be optimized within the space and aspect ratio constraints: the input voltage (V_{in}), total length and width of the device, device thickness, length of the interdigitated fingers, and nominal gap between fingers. Two formal optimizations were performed in Matlab to determine the optimal design parameters: one with the mechanical stops placed such that the minimum dielectric gap is 0.25 μm, and another such that the minimum gap is 0.5 μm. The optimal design parameters and output power are summarized in Table 3.

 Copyright © 2002 by ASME

Vars	Description of Variable	0.25 µm min gap	0.5 µm min gap
w	Width of shuttle mass	10 mm	10 mm
L	Length of shuttle mass	9 mm	8 mm
L_{fin}	Length of fingers	530 µm	1.2 mm
t	Device thickness	200 µm	200 µm
Vin	Input voltage	10 V	10 V
gap	Nominal dielectric gap	50 µm	50 µm
Pout	Output power	116 µW	101 µW

Table 3: Optimal design parameters and power output for an in-plane gap closing design.

The objective function for the optimization is the output power determined by dynamic simulations using Eqs. (1a, 2, 12-14). The optimal power output for a 0.25 µm minimum gap is 116 $\mu W/cm^3$ and for a 0.5 µm minimum gap is 101 $\mu W/cm^3$. Devices are currently in fabrication based on the optimized design parameters shown in Table 3. Figure 13 shows a SEM of a preliminary device that has been fabricated and is currently being tested. The SEM shows only a corner of the device highlighting the interdigitated fingers that form the variable capacitor and one of the flexures.

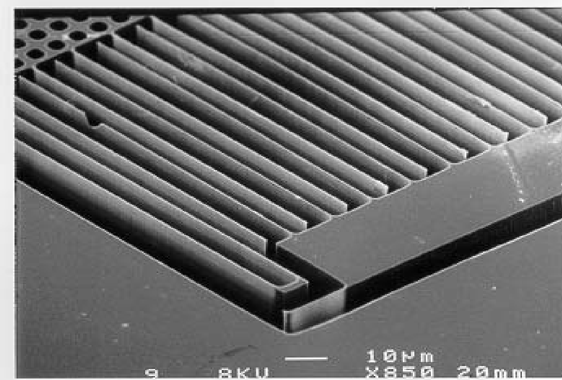

Figure 13. SEM of a corner of an in-plane gap closing prototype device.

8. CONCLUSIONS

There has recently been an increasing interest in technologies and ideas to scavenge or harvest small bits of energy from the environment for use by low power electronics. The interest is fueled by the decreasing size and power consumption of electronics that make a small self-powered wireless device plausible. This work has explored the use of low level mechanical vibrations as a power source for wireless sensor nodes. Specifically, electrostatic converters fabricated using silicon MEMS technology have been investigated because of the ability to closely integrate such converters with silicon based microelectronics. Three potential design concepts were considered and evaluated. Models were developed for each of the design concepts. Simulations and practical considerations confirm that the in-plane gap closing type converter is the preferable topology. A formal optimization based on dynamic simulations revealed that an output power density of 116 $\mu W/cm^3$ is possible from a vibration source of 2.25 m/s^2 at 120 Hz. This vibration source very closely matches the casing of a microwave oven, which falls about in the middle, in terms of energy potential, of several measured sources of low level vibrations. Test devices have been designed for a DRIE process that etches MEMS structures into the top layer of a SOI wafer. The devices are currently in the fabrication stage.

ACKNOWLEDGMENTS

The authors wish to acknowledge the support of this work by DARPA on grant no. F29601-99-1-0169 entitled, "Communication/Computation Piconodes for Sensor Networks". The work was also partially supported by the Department of Energy under the Integrated Manufacturing and Processing Fellowship. The authors also wish to thank Professor Jan Rabaey for his helpful discussion and input.

REFERENCES

[1] J. M. Rabaey, M. J. Ammer, J. L. da Silva Jr., D. Patel, and S. Roundy, "PicoRadio Supports Ad Hoc Ultra Low-Power Wireless Networking," *Computer*, vol.33, (no.7), IEEE Comput. Soc, July 2000. p.42-8

[2] A. Chandrakasan, R. Amirtharajah, J. Goodman, and W. Rabiner, "Trends in low power digital signal processing," *Proceedings of the 1998 IEEE International Symposium on Circuits and Systems*, 1998, pp. 604-7.

[3] M. Stordeur and I. Stark, "Low Power Thermoelectric Generator – self-sufficient energy supply for micro systems" *16th International Conference on Thermoelectrics*, 1997, pp. 575 – 577.

[4] C. B. Williams and R. B. Yates, "Analysis of a micro-electric generator for microsystems," *Proc. Transducers 95/Eurosensors IX*, (1995) 369 – 372.

[5] S. Meninger, J. O. Mur-Miranda, R. Amirtharajah, A. P. Chandrakasan, and J. H. Lang, "Vibration-to-Electric Energy Conversion," *IEEE Trans. VLSI Syst.*, 9 (2001) 64-76.

[6] N. S. Shenck and J. A. Paradiso, "Energy Scavenging with Shoe-Mounted Piezoelectrics," *IEEE Micro*, 21 (2001) 30-41.

[7] R. Amirtharajah and A. P. Chandrakasan, "Self-Powered Signal Processing Using Vibration-Based Power Generation," *IEEE J. Solid-State Circuits*, 33 (1998) 687-695.

[8] N. G. Elvin, A. A. Elvin, and M. Spector, "A self-powered mechanical strain energy sensor," *Smart Materials and Structures*, 10 (2001) 293 – 299.

[9] V. H. Schmidt, "Theoretical Electrical Power Output per Unit Volume of PVF_2 and Mechanical-to-Electrical Conversion Efficiency as Functions of Frequency" *Proceedings of the Sixth IEEE International Symposium on Applications of Ferroelectrics*, (1986) 538-42.

[10] U. Srinivasan, D. Liepmann, and R.T. Howe, "Microstructure to substrate self-assembly using capillary forces." *Journal of Microelectromechanical Systems*, vol.10, (no.1) (2001) 17-24.

[11] T-R. Hsu, "Packaging Design of Microsystems and Meso-Scale Devices," *IEEE Transactions on Advanced Packaging*, vol. 23 (no. 4) (2000) 596 – 601.

[12] Y. T. Chang and L. Lin, "Localized Silicon Fusion and Eutectic Bonding for MEMS Fabrication and Packaging," Journal of Microelectromechanical Systems, vol. 9 (no. 1) (2001) 3 – 8.

 Copyright © 2002 by ASME